Nonlinear Analysis: Modelling and Control, Vilnius, IMI, 1998, No 3

PROPERTIES OF GENERALIZED SYNCHRONIZATION OF CHAOS

K. Pyragas
Semiconductor Physics Institute, A.Goštauto 11, 2600 Vilnius, Lithuania

Abstract

A review of recent ideas in the field of generalized synchronization of chaos is presented. This field is concerned with a generalization of the concept of conventional (identical) chaotic synchronization to the case of one-way coupled nonidentical chaotic systems. Generalized synchronization is taken to occur if, ignoring transients, the response system becomes uniquely determined by the current state of the driving system, i.e., all trajectories in the phase space are attracted to a complex synchronization manifold that may have a fractal structure. Different tools for detecting and analyzing the properties of this type of synchronization are discussed.

INTRODUCTION

The cooperative behavior of coupled dynamical systems is becoming to an important field of nonlinear dynamics. Synchronization effects in systems with periodic behavior are widely used in engineering, for example, for improvement of the line width of a high-power generator with the help of a low-power generator having a narrower spectral line.

In recent years, the synchronization of coupled chaotic systems has become an area of active research. The motivation for these investigations derived from possible applications of this phenomenon to secure communications [1], the long-term prediction of chaotic systems [2], controlling chaos [3], the model verification of nonlinear dynamics [4], or the estimation of model parameters [5]. Also, understanding the synchronization process is important for efficient control of the spatiotemporal chaos that occurs in various complex systems such as laser arrays [6] or cardiac systems [7].

A generic feature of nonlinear systems exhibiting chaotic motion is extreme sensitivity to initial conditions. This feature, known as the "butterfly effect", would seem to defy synchronization among dynamical variables in coupled chaotic

systems. Nonetheless, coupled systems with certain properties of symmetry may exhibit synchronized chaotic motions. Most frequently a situation is studied where the complete system consists of *coupled identical subsystems*. Many different examples of this type have been introduced [2, 8, 9]. In these cases, the synchronization is easy to detect. It appears as an actual equality of the corresponding variables of the coupled systems as they evolve in time. Geometrically, this implies a collapse of the overall evolution onto the identity hyperplane in the full phase space. As suggested in [10], we refer to this type of synchronization as an *identical synchronization* (IS).

A more complicated situation arises when *coupled non-identical chaotic systems* are investigated. For essentially different chaotic systems, the phase space does not contain any trivial invariant manifolds from which one can expect a collapse of the overall evolution. The central questions in this case are (i) how to generalize a mathematical definition of chaotic synchronization for such systems and (ii) how to detect it in a real experimental situation. Recently, two approaches have been suggested in order to answer these questions. One of them [11] uses the concept of an analytical signal and introduces an instantaneous phase and amplitude for the chaotic process. The synchronization appears as locking of the phases of the coupled systems, while the amplitudes remain uncorrelated. This type of synchronization is identified as a *phase synchronization*. Another approach [12] is based on the concept of the functional relationship between the variables of the coupled subsystems. It becomes particularly attractive in connection with a recent publication of Rulkov *et al.* [13]. They restricted their consideration to the case of forced synchronization. This means that the full system consists of an *autonomous driving* subsystem that is one-way linked to a *response* subsystem. *Generalized synchronization* (GS) is taken to occur if, ignoring transients, the response $Y(t)$ is uniquely determined by the current drive state $X(t)$. That is, $Y(t) = \Phi(X(t))$, where Φ is a mapping that takes the trajectories $X(t)$ of the attractor in the driving space to the trajectories $Y(t)$ in the response space. For non-identical driving and response systems, the map differs from identity, which complicates the detection of GS. To recognize GS in a real experimental situation, Rulkov *et al.* [13] suggested a practical algorithm based on the assumption that Φ is a *smooth* (differentiable) map. The algorithm was tested on artificially constructed examples with an *a priori* known map Φ. Subsequent progress of GS theory was achieved in recent publications [10, 14, 15, 16, 17, 18]. Depending on the properties of the map Φ, two different types of GS were discovered [16], namely, *strong synchronization* (SS) and *weak synchronization* (WS), which are characterized by a *smooth* and a *nonsmooth*

(fractal) map Φ, respectively.

The main goal of this chapter is to review the recent ideas of GS theory. Particularly, we focus on different numerical and experimental tools for detecting GS and analyzing its properties. In Sec. 1, we briefly describe the main ideas defining the concept of GS. In Sec. 2, we introduce some numerical characteristics to estimate the properties of the synchronization manifold. With the help of various examples, we show that GS may appear in two different states, referred to as WS and SS. In Sec. 3, we show that at the threshold of WS the system exhibits a new type of on-off intermittency. Unlike the conventional on-off intermittency, where the system dynamics is determined by the escape of trajectories from an unstable smooth hyperplane, this intermittency is characterized by the escape of trajectories from an unstable fractal manifold. Sec. 4 is devoted to the detection of GS from time series analysis. A special algorithm for estimating conditional Lyapunov exponents from two scalar data sets, one taken from the driving system and the other taken from the response system, is described. Sec. 5 contains the conclusions of our review.

1. GENERALIZED SYNCHRONIZATION OF CHAOS

Let us consider one-way coupled chaotic systems of the following general form (master-slave configurations or systems with a skew product structure):

$$\dot{X} = F(X), \tag{1}$$

$$\dot{Y} = G(Y, X). \tag{2}$$

Here $X \equiv \{x_1, x_2, \ldots, x_d\}$ is a d-dimensional state vector of the driving system and $Y \equiv \{y_1, y_2, \ldots, y_r\}$ is an r-dimensional state vector of the response system. F and G define the vector fields of the driving and response systems.

One can show [10, 14] that there exists some mapping Φ (not necessarily smooth [16]) between X and Y if, under the action of driving perturbations, the response system "forgets" its initial conditions, i.e., when the response system becomes a *stable system* [19]. This suggests an auxiliary system approach [14] as a tool for detecting GS in an experiment. According to this approach, it is supposed that we are able to construct an auxiliary response system Y' that is identical to Y and to link it to the driving system X in the same way that Y is linked to X[1]:

$$\dot{Y'} = G(Y', X). \tag{3}$$

[1] The related problem of synchronizing identical systems that are driven by random noise has been considered in [20]

Due to the identity of the original [Eq. (2)] and the auxiliary [Eq. (3)] response systems, they may exhibit IS. GS between X and Y occurs if there is IS between Y and Y'. To show [16] that IS between Y and Y' results in the relationship $Y = \Phi(X)$, let us denote the solution of Eqs. (1), (2) by $X(t) = \Psi_x(X_0, t)$ and $Y(t) = \tilde{\Psi}_y(X_0, Y_0, t)$, where $X = X_0$ and $Y = Y_0$ are the initial conditions at $t = 0$. If the driving dynamics is invertible, $X_0 = \Psi_x(X(t), -t)$, the response solution can be rewritten as $Y(t) = \tilde{\Psi}_y(\Psi_x(X(t), -t), Y_0, t) \equiv \Psi_y(X(t), Y_0, t)$. IS between Y and Y' implies $\lim_{t\to\infty} \|Y - Y'\| = \lim_{t\to\infty} \|\Psi_y(X(t), Y_0, t) - \Psi_y(X(t), Y_0', t)\| = 0$ for arbitrary initial conditions Y_0 and Y_0' taken in some region of Y space. From this it follows that Ψ_y is asymptotically independent of Y_0. As $t \to \infty$, Ψ_y is also independent of the explicit time t. Indeed, let $\tilde{Y_0'} = \Psi_y(X(\tilde{t}), Y_0', \tilde{t})$ be the state of the system Y' at an intermediate time $\tilde{t} < t$. Then the state of the system Y' at time t can be expressed as $Y'(t) = \Psi_y(X(t), \tilde{Y_0'}, t - \tilde{t})$ and the synchronization condition becomes $\lim_{t\to\infty} \|\Psi_y(X(t), Y_0, t) - \Psi_y(X(t), \tilde{Y_0'}, t - \tilde{t})\| = 0$ for any $\tilde{t} < t$. It follows that as $t \to \infty$, Ψ_y is independent of both Y_0 and the explicit time t. Thus, in the limit $t \to \infty$, we obtain a relationship between X and Y in the form $Y = \lim_{t\to\infty} \Psi_y(X(t), Y_0, t) \equiv \Phi(X(t))$.

GS guarantees that the asymptotic dynamics of the response system is independent of its initial conditions and is completely determined by the driving system. Geometrically, this implies a collapse of the overall evolution onto a stable synchronization manifold $M = \{(X, Y) : \Phi(X) = Y\}$ in the full phase space of the two systems $X \oplus Y$. It is easy to show [14] that the linear stability of the identity manifold $Y' = Y$ in the extended phase space $X \oplus Y \oplus Y'$ is equivalent to the linear stability of the manifold $M = \{(X, Y) : \Phi(X) = Y\}$ in the original $X \oplus Y$ phase space. The linear equations that govern the evolution of the quantities $\delta Y = Y - \Phi(X)$ and $\delta Y' = Y - Y'$ are equivalent:

$$\dot{\delta Y} = D_Y G(Y, X(t)) \delta Y, \tag{4}$$

$$\dot{\delta Y'} = D_Y G(Y, X(t)) \delta Y'. \tag{5}$$

Here $D_Y G$ denotes the Jacobian matrix of the response system with respect to the Y variable, where $Y = Y(t) = \Phi(X(t))$ is defined by Eqs. (1), (2). Therefore, if the manifold of synchronized motions in $X \oplus Y \oplus Y'$ is linearly stable for $\delta Y' = Y - Y'$, than it is linearly stable for $\delta Y = Y - \Phi(X)$ and *vice versa*. Note that the linearized equations for $\delta Y' = Y - Y'$ are identical to the equation that defines the *conditional Lyapunov exponents* (CLEs) for the response system $\lambda_1^R \geq \lambda_2^R \geq \ldots \geq \lambda_r^R$ [8]. Both

manifolds $Y' = Y$ and $Y = \Phi(X)$ are stable when all CLEs are negative. Thus, the condition of GS is $\lambda_1^R < 0$.

We have thus demonstrated that to study the transition to GS, the analysis of the stability of the synchronization manifold in the space $X \oplus Y$, which in general may have a very complex shape $Y = \Phi(X)$, can be replaced by the analysis of the stability of the simple identity manifold $Y = Y'$ in $Y \oplus Y'$ space.

2. WEAK AND STRONG SYNCHRONIZATION

Properties of the synchronization manifold

Note that IS between Y and Y' does not guarantee the smoothness of Φ [16]. The synchronization manifold $M = \{(X, Y) : \Phi(X) = Y\}$ can have a fractal structure. Ding *et al.* [21] have illustrated that nonsmooth (fractal) maps do not preserve the dimension of strange attractors. As a simple example of this type, let us consider the Weierstrass function $y = F_w(x) \equiv \sum_{n=1}^{\infty} \cos(n^\beta x)/n^\alpha$. It specifies a continuous (C^0) but non-differentiable map of points on the x-axis (with the dimension equal to 1) to points on the Weierstrass curve $x \to [x, y = F_w(x)]$ with a fractal dimension between 1 and 2 for typical values of α and β satisfying $1 < \alpha < \beta$. Recently, Sauer and Yorke [22] gave a criterion for dimension preservation. They provide a theorem which shows that continuously differentiable (C^1) maps preserve the dimension of strange attractors.

Thus, depending on the properties of the synchronization manifold, GS can be subdivided into two types. For the continuous C^0 but nonsmooth map Φ, the global dimension of the strange attractor d^G in the whole phase space $X \oplus Y$ is larger than the dimension of the driving attractor d^D in the X subspace, $d^G > d^D$. We refer to this type of synchronization as WS. For smooth Φ with degree of smoothness C^1 or higher, we expect that the response system does not have effect on the global dimension, i.e., $d^G = d^D$. This type of synchronization we call SS. Obviously, IS is a particular case of SS.

The threshold of SS can be estimated from the Kaplan-Yorke conjecture [23], in the same way that Badii *et al.* determined the condition at which a linear low-pass filter does not influence the dimension of filtered chaotic signals [24]. Note that for systems with a skew product structure described by Eqs. (1), (2), the CLEs represent a part of the whole Lyapunov spectrum $\lambda_1, \lambda_2, \ldots, \lambda_{r+d}$ of this system. The remainder of this spectrum consists of Lyapunov exponents $\lambda_1^D \geq \lambda_2^D \geq \ldots \geq \lambda_d^D$ of the driving system (1). In other words, to obtain the whole spectrum of Lyapunov exponents of system (1), (2) in the usual (descending) order,

$\lambda_1 \geq \lambda_2 \geq \ldots \geq \lambda_{r+d}$, the combined spectrum of the driving Lyapunov exponents and the CLEs $\lambda_1^D, \lambda_2^D, \ldots, \lambda_d^D, \lambda_1^R, \lambda_2^R, \ldots, \lambda_r^R$ have to be resorted in order of their numerical size. If the whole spectrum of the Lyapunov exponents is known, then one can extract information about the properties of the synchronization manifold. Using the Kaplan-Yorke conjecture [23], the dimensions d^G and d^D can be estimated as follows:

$$d_\lambda^G = l_G + \frac{1}{|\lambda_{l_G+1}|} \sum_{l=1}^{l_G} \lambda_l \,, \tag{6}$$

$$d_\lambda^D = l_D + \frac{1}{|\lambda_{l_D+1}^D|} \sum_{l=1}^{l_D} \lambda_l^D \,, \tag{7}$$

where l_G and l_D are the largest integers for which the corresponding sums over l are nonnegative. The lower index λ indicates that these dimensions are calculated from the Lyapunov exponents. The global Lyapunov dimension is independent of the response system ($d_\lambda^G = d_\lambda^D$) at the condition [16] $\lambda_1^R < \lambda_{l_D+1}^D$. If this condition is fulfilled and relations (6) and (7) are valid, we have SS.

The smoothness of Φ can be also estimated by a more direct criterion, namely, by determining the mean local "thickness" σ of the synchronization manifold [16]. Let us consider a set of points $[X_i]_{i=1}^N \equiv [X(t_i)]_{i=1}^N$ and $[Y_i]_{i=1}^N \equiv [Y(t_i)]_{i=1}^N$ in the spaces of the coupled systems coming from finite segments of trajectories sampled at the moments $t_i = i\Delta t$. Pick an arbitrary point X_k and find its $N_n > d\,r$ neighbors X_j whose distance from X_k is less than ϵ; $\|X_j - X_k\| < \epsilon$, $j = 1, \ldots, N_n$. Suppose that, for small ϵ, the points X_j are related to their images Y_j by a linear map $Y_j - Y_k = A_k\,(X_j - X_k)$, where A_k is a $d \times r$ matrix, whose elements can be determined by a least-squares fit. Then the square of the local thickness of the synchronization manifold at the point X_k can be estimated as $\sigma_k^2 = \sum_{j=1}^{N_n} [Y_j - Y_k - A_k(X_j - X_k)]^2$. The mean thickness σ is obtained by averaging the local values, $\sigma = \sqrt{\sum_{k=1}^N \sigma_k^2 / N}$.

Now we illustrate some properties of GS with specific examples. As usual in such problems, we start with discrete time systems. At first we consider coupled identical subsystems which can exhibit IS and show that even in this case WS appears for coupling strength below the threshold of IS. The last example illustrates GS in essentially different coupled time-continuous systems.

Numerical examples

Coupled Logistic Maps. Let us consider a simple example of two one-way coupled identical one-dimensional logistic maps:

$$x(i+1) = f(x(i)), \tag{8}$$

$$y(i+1) = f(y(i)) + k\{f(x(i)) - f(y(i))\} \tag{9}$$

with $f(x) = 4ax(1-x)$ and $a = 1$. Here Eqs.(8) and (9) describe the driving and response systems, respectively, k is the coupling strength. At $0 < k < 1$, the coupling term in Eq.(9) preserves the global stability of the response system, since $0 < (1-k)f(y(i)) + kf(x(i)) < 1$ at any $x(i)$ and $y(i)$ lying in the interval $[0, 1]$. To observe GS, we consider an auxiliary response system

$$y'(i+1) = f(y'(i)) + k\{f(x(i)) - f(y'(i))\} \tag{10}$$

identical with the original response system (9), but having a different initial condition than that of system (9). We emphasize that this system does not influence the dynamics of the original response and driving subsystems described by Eqs. (8), (9). It serves only to detect the properties of the system (8), (9).

At any coupling strength k, Eqs. (8), (9) have an invariant manifold $y = x$ and, hence, admit IS. The case of identical systems is interesting, since it provides a simple criterion for SS. SS for such systems is equivalent to IS. Indeed, the identity diagonal $y = x$ is an invariant manifold of the system (8), (9). If it is a stable manifold, the variables of the response and driving systems are related by the identity map $y(i) = x(i)$, which obviously is smooth. Thus, SS can be simply detected as IS between the driving and response systems.

Fig. 1 shows the phase portraits of the system for the logistic map in x-y and y-y' coordinates at $a = 1$ and for various values of parameter k. With the increase of k, synchronization occurs first between y and y' and, later on, between x and y. Thus, GS in the form of WS is observed even for identical systems, and it precedes SS. The thresholds of WS and SS are determined by two different Lyapunov exponents, namely, the CLE

$$\lambda^R = \ln(1-k) + \lim_{n\to\infty} \frac{1}{n} \sum_{i=1}^{n} \ln |f'(y(i))| \tag{11}$$

defining the stability of the invariant manifold $y' = y$, and the transverse Lyapunov exponent of the identity manifold $y = x$

$$\lambda^I = \ln(1-k) + \lim_{n\to\infty} \frac{1}{n} \sum_{i=1}^{n} \ln |f'(x(i))|. \tag{12}$$

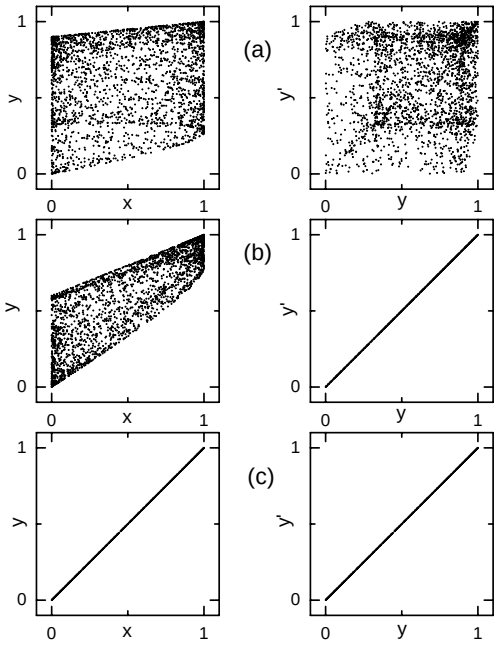

Fig. 1. x-y and y-y' phase portraits of coupled logistic maps for various values of the coupling strength k: (a) k=0.1, unsynchronized state; (b) k=0.4, WS; (c) k=0.6, SS.

The dependence of these exponents on k is shown in Fig. 2(a). $\lambda^R(k)$ becomes zero at two characteristic values of the coupling strength k_w and k_s, corresponding to the thresholds of WS and SS, respectively. Above the latter threshold $k > k_s$, these two exponents coincide, $\lambda^I(k) = \lambda^R(k)$. For the logistic map, Eq. (12) transforms to $\lambda^I(k) = \ln(1-k) + \lambda^D$, where $\lambda^D = \ln 2$ is the Lyapunov exponent of the driving system and the threshold of SS is equal to $k_s = 1 - \exp(-\lambda^D) = 0.5$.

In a real experiment, IS between the systems Y and Y' will be partially disturbed by noise and the small mismatch between the parameters of these systems. These factors will result in a finite amplitude of the deviation $Y' - Y$. Numerical analysis shows that the r.m.s. of this deviation $s_{RR} = \sqrt{\langle (Y'-Y)^2 \rangle}$ depends on the amplitude of the noise α_n by a power law $s_{RR} \propto \alpha_n^\gamma$. In the case of Eqs. (8), (9) and (10), $\gamma \approx 0.12$ for WS and $\gamma = 1$ for SS [see the insert in Fig. 2(a)]. The same scaling laws are observed for s_{RR} *vs* Δa, where Δa is the

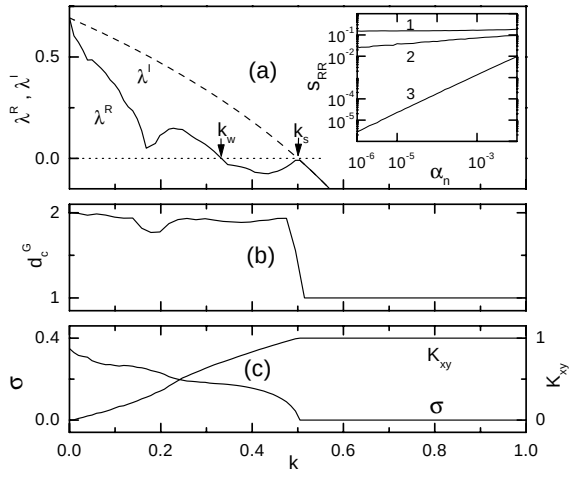

Fig. 2. (a) Conditional λ^R and identity λ^I Lyapunov exponents, (b) correlation dimension d_c of the attractor in the x-y plane, (c) thickness σ and cross correlator K_{xy} for coupled logistic maps as functions of coupling strength k. λ^R and λ^I are calculated from Eqs. (11) and (12), respectively. d_c and σ are determined from N=50000 data points $(x(i), y(i), i = 1, \ldots, N)$. The insert in (a) shows the deviation s *vs* the amplitude of noise α_n: (1) unsynchronized state at $k = 0.3$; (2) WS at $k = 0.4$; (3) SS at $k = 0.6$. At every iteration, random numbers uniformly distributed in the interval $[-\alpha_n/2, \alpha_n/2]$ have been added to the variables of Eqs. (8), (9) and (10).

deviation between the parameters of the systems y and y' [$a = 1$ for Eqs. (8), (9) and $a = 1 - \Delta a$ for Eq. (10)]. Thus, WS is much more sensitive ($\gamma < 1$) to noise and parameter deviations than SS ($\gamma = 1$).

WS observed with the help of an auxiliary response system y' may show no evidence in x-y coordinates. At $k_w < k < k_s$, there exists a relationship $y = \Phi(x)$, however, the map Φ is nonsmooth and has a fractal structure [Fig. 1(b), left]. The global correlation dimension [25] d_c^G of an attractor lying in the x-y plane does not exhibit any characteristic changes at the threshold k_w [Fig. 2(b)]. An abrupt dimension decrease is observed only at the threshold k_s, where Φ is turned to identity. At the threshold of WS, there are no characteristic changes in the cross-correlator K_{xy} between x and y variables [Fig. 2(c)], although here this correlation is rather large, $K_{xy}(k_w) \approx 0.71$. WS similarly shows no evidence in the mean local thickness σ of the synchronization manifold [Fig. 2(c)]. The thickness σ decreases

abruptly only at $k = k_s$, like the dimension d_c^G. At $k > k_s$, Φ becomes a smooth map; the thickness σ turns to zero and the global dimension d_c^G becomes equal to the dimension d_c^D of the strange attractor of the driving system, $d_c^G = d_c^D = 1$.

Although this example is based on an noninvertable logistic map, similar effects are observed in coupled invertable Hénon maps.

Coupled Hénon Maps. The second example represents two identical one-way coupled invertable Hénon [26] maps

$$\begin{pmatrix} x_1(i+1) \\ x_2(i+1) \end{pmatrix} = \begin{pmatrix} f[x_1(i), x_2(i)] \\ bx_1(i) \end{pmatrix} \tag{13}$$

$$\begin{pmatrix} y_1(i+1) \\ y_2(i+1) \end{pmatrix} = \begin{pmatrix} (1-k)f[y_1(i), y_2(i)] + kf[x_1(i), x_2(i)] \\ by_1(i) \end{pmatrix} \tag{14}$$

where $f[x_1, x_2] = 1 - ax_1^2 + x_2$, $a = 1.4$, $b = 0.3$, and k is the control parameter defining the coupling strength. At any k, this system (like the to a previous example) has an invariant manifold $Y = X$ and, hence, admits IS which is equivalent to SS. IS appears when the identity manifold $Y = X$ becomes stable. The linear stability of this manifold is described by the variational equations

$$\begin{pmatrix} \delta y_1(i+1) \\ \delta y_2(i+1) \end{pmatrix} = \begin{pmatrix} -2(1-k)x_1(i) & 1 \\ b & 0 \end{pmatrix} \begin{pmatrix} \delta y_1(i) \\ \delta y_2(i) \end{pmatrix} \tag{15}$$

defining the two transverse Lyapunov exponents λ_1^I and λ_2^I. The dependence of the maximal transverse Lyapunov exponent λ_1^I on k is shown in Fig. 3. It becomes negative when k exceeds some threshold $k > k_3 \approx 0.34$. Before reaching this threshold, the system exhibits GS in the form of WS. This conclusion can be made by analyzing the CLEs of the response system. They are determined from the variational equations

$$\begin{pmatrix} \delta y_1'(i+1) \\ \delta y_2'(i+1) \end{pmatrix} = \begin{pmatrix} -2(1-k)y_1(i) & 1 \\ b & 0 \end{pmatrix} \begin{pmatrix} \delta y_1'(i) \\ \delta y_2'(i) \end{pmatrix} \tag{16}$$

defining the dynamics of small deviations $\delta Y' = Y - Y'$, where Y' is the variable of the auxiliary response system constructed in accordance with Eq. (14). The dependence of the maximal CLE λ_1^R on k is also presented in Fig. 3. In the general case, the exponent λ_1^R differs from λ_1^I when the driving and response systems are not synchronized in the sense of IS. They coincide only in the domain of the control parameter k, where $\lambda_1^I(k) < 0$. If we suppose that the identity plane $Y = X$ is the only invariant smooth manifold of the system, the conditions of WS can be expressed as $\lambda_1^R(k) < 0$, $\lambda_1^I(k) > 0$. The first condition guarantees the existence of

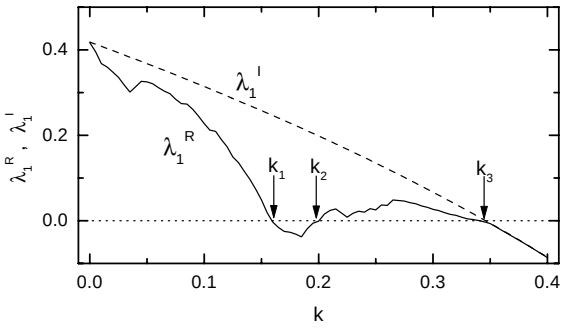

Fig. 3. (a) Maximal conditional λ_1^R and identity λ_1^I Lyapunov exponents as functions of the coupling strength k for one-way coupled Hénon maps. The interval $k_1 < k < k_2$ corresponds to WS. At $k > k_3$, the systems (13), (14) exhibit identical behavior corresponding to SS.

a stable synchronization manifold and the second condition shows that the smooth identity manifold $Y = X$ is unstable.

Thus, WS is observed in the interval $k \in [k_1, k_2]$, $k_1 \approx 0.16$, $k_2 \approx 0.20$. Here, the maximal CLE is negative, while the maximal transverse Lyapunov exponent is positive. This means that the systems Y and Y' are synchronized in the sense of IS and there is no IS between X and Y.

Coupled Rössler and Lorenz systems. As a third example, we present GS in essentially different time-continuous systems:

$$\frac{d}{dt}\begin{pmatrix} x_1 \\ x_2 \\ x_3 \end{pmatrix} = \alpha \begin{pmatrix} -x_2 - x_3 \\ x_1 + 0.2x_2 \\ 0.2 + x_1x_3x_1 - 5.7x_3 \end{pmatrix}, \tag{17}$$

$$\frac{d}{dt}\begin{pmatrix} y_1 \\ y_2 \\ y_3 \end{pmatrix} = \begin{pmatrix} 10(-y_1 + y_2) \\ by_1 - y_2 - y_1y_3 \\ y_1y_2 - 8/3y_3 \end{pmatrix} + k \begin{pmatrix} 0 \\ x_2 \\ 0 \end{pmatrix} \tag{18}$$

. These equations describe the coupling of the Rössler [27] [Eqs. (17), driving] and the Lorenz [28] [Eqs. (18), response] systems. The multiplier $\alpha = 6$ is introduced to control the characteristic time scale of the driving system. Here the parameter b is chosen to be $b = 28$. The perturbation kx_2 is applied only to the second equation of the Lorenz system and does not contain any feedback term. In addition to Eqs. (17), (18) we consider an auxiliary response system which is equivalent to the system of Eqs. (18) except that the variables y_i are replaced with y_i'.

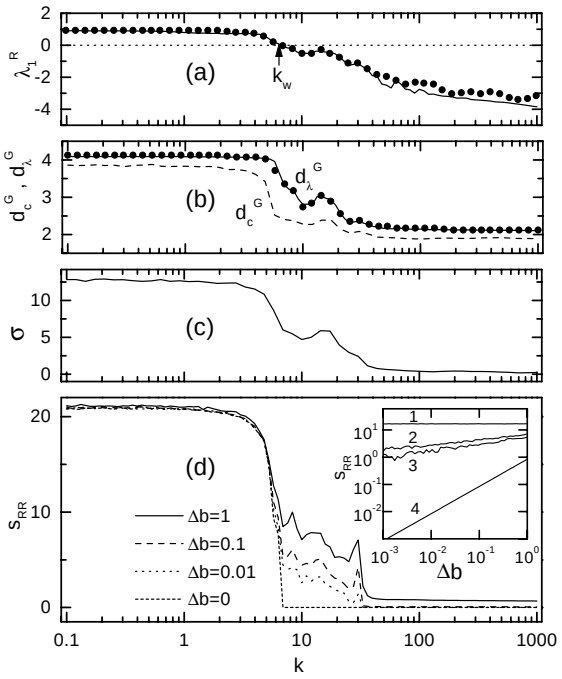

Fig. 4. (a) Maximal CLE λ_1^R, (b) global correlation d_c^G and Lyapunov d_λ^G dimensions, (c) thickness σ, and (d) deviation s for coupled Rössler and Lorenz systems as functions of the coupling strength k. d_c and σ are calculated from N=50000 data points $(X(i\Delta t),\ Y(i\Delta t), i = 1, \ldots, N)$ with Δt=0.5. The points in (a) and (b) show the maximal CLE and global Lyapynov dimension, respectively, calculated from time series (see Sec. 4. The insert in (c) shows s *vs* the deviation of the parameter Δb: (1) unsynchronized state at k=5; (2) WS at $k = 10$; (3) WS at $k = 20$; (4) SS at $k = 50$.

Despite the lack of any symmetry in Eqs. (17), (18) admitting IS, this system can exhibit GS. As in the previous examples, GS can easily be detected as IS between Y and an auxiliary response system Y'. The threshold of GS is determined by $\lambda_1^R(k) = 0$ and is equal to $k_w \approx 6.66$ [Fig. 4(a)]. In this model, the onset of GS is characterized by a considerable decrease of both the dimension [Fig. 4(b)] and the thickness of the map [Fig. 4(c)]. However, the mean local thickness of the synchronization manifold remains rather large. This means that here we actually have the transition to WS. In the case of a driving system presented by a three-dimensional flow, the condition of SS defining the equality of the global and driving Lyapunov dimensions $d_\lambda^G = d_\lambda^D$ becomes $\lambda_1^R(k) < \lambda_3^D$. For the system of Eqs. (17), we have $\lambda_1^D \approx 0.41$, $\lambda_2^D = 0$, $\lambda_3^D \approx -37.66$ and the driving Lyapunov dimension is equal to $d_\lambda^D = 2 + \lambda_1^D/|\lambda_3^D| \approx 2.01$. Because of the large negative value of λ_3^D, the condition $\lambda_1^R(k) < \lambda_3^D$ is not achieved even for very large $k \approx 1000$, and we have WS for all $k > k_w$. Although the rigorous criterion of WS $d_\lambda^G(k) > d_\lambda^D$ is fulfilled for all $k > k_w$, the global dimension goes down to a value approximately equal to the driving dimension at $k \gtrsim 40$. Here, the global dimension is $d_\lambda^G(k) = 2 + \lambda_1^D/|\lambda_1^R(k)|$ and, since $\lambda_1^D/|\lambda_3^D| \ll 1$ and $\lambda_1^D/|\lambda_1^R \ll 1$, we have $d_\lambda^G(k) \approx d_\lambda^D \approx 2$. Therefore, one can conclude that the synchronization manifold is almost smooth at $k \gtrsim 40$. This conclusion is confirmed by the dependence of the mean local thickness σ on k; at $k \gtrsim 40$, the thickness becomes very small. Thus, the region $k \gtrsim 40$ can be interpreted as a domain of not fully developed SS.

Fig. 4(d) shows the influence of a small mismatch between the parameters of systems Y and Y' in the case of Eqs. (17), (18). The parameter b of the system Y' is replaced by $b + \Delta b$. For finite Δb, the two pronounced thresholds in the dependence $s_{RR} = \sqrt{\langle (Y' - Y)^2 \rangle}$ *vs* k related to the onset of WS and not fully developed SS are observed. The last threshold is conditioned by the different sensitivities of the smooth and nonsmooth synchronization manifold to the parameter deviation; $s_{RR} \propto \Delta b^\gamma$ with $\gamma \approx 0.2$ for $k_w < k < 40$ and $\gamma \approx 1$ for $k \gtrsim 40$. These different scaling laws ($\gamma = 1$ for the smooth manifold and $\gamma < 1$ for the nonsmooth manifold) can serve as a practical criterion for estimating the smoothness of the synchronization manifold in experiments.

3. ON-OFF INTERMITTENCY

A recent publication of Platt, Spiegel, and Tresser [29] has inspired great interest to a particular behavior of nonlinear systems known as on-off intermittency. This behavior derives its name from the characteristic two-state nature of the

intermittent signal. The "off" (laminar) state is nearly constant and can remain so for very long periods of time. The "on" state is a burst, departing quickly from, and returning quickly to, the off state. Such behavior occurs in dynamical systems with certain symmetry properties. The chaotic attractor of such systems lies on a smooth invariant manifold (usually a hyperplane) having a lower dimension than the dimension of the full phase space. This attractor may become a repeller at the blow-out bifurcation [30]. The on-off intermittency is observed just above this bifurcation threshold. Initially, this intermittency was discovered numerically in the system of coupled identical chaotic maps [31]. Later, it was investigated in various mathematical models, such as a set of coupled ordinary differential equations [29], random maps [32], and random map lattices [33], as well as various physical systems, such as particle motion in a symmetrical potential [34], electronic circuits [35], and high power ferromagnetic resonance [36].

Here, we show [18] that the class of nonlinear chaotic systems exhibiting on-off intermittency can be essentially extended. On-off intermittency may appear in systems that do not possess any trivial invariant manifolds. It may occur in any dynamical system consisting of two one-way coupled chaotic subsystems at the threshold of WS.

Let us illustrate this with the simple example of two one-way coupled logistic maps [Eqs. (8), (9)] considered in Sec. 2. In the region of coupling strength $k_w < k < k_s$, we have IS between the original and auxiliary response systems $y(i) = y'(i)$ and have no IS between the driving and original response systems $y(i) \neq x(i)$. This corresponds to WS between the driving x and original response y systems. Here, the identity manifold $y = x$ is unstable and the overall dynamics in the x-y plane collapses to another invariant synchronization manifold $M = \{(x, y) : y = \Phi(x)\}$ that has a fractal structure. This manifold is shown in Fig. 5(a) (left) just above the threshold of WS. The IS between y and y' [Fig. 5(a), right] testifies to the stability of this manifold. Just below the threshold of WS ($k < k_w$), the CLE becomes positive, $\lambda^R(k) > 0$. This means that the fractal synchronization manifold responsible for WS becomes unstable. Close to the threshold, we can expect that the system spends a long time in the vicinity of the manifold and experiences short bursts away from this manifold. Fig. 5(b) shows the x-y and y-y' phase portraits just below the threshold of WS. The expected intermittent behavior is not seen in x-y coordinates. However, it can be detected with the help of an auxiliary response system (10). A typical structure for intermittent behavior is seen in y-y' coordinates. Fig. 6 illustrates the dynamics of $y(i)$ and the difference $y(i) - y'(i)$

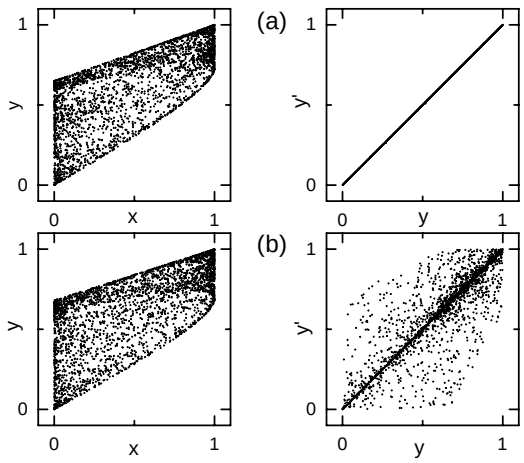

Fig. 5. x-y and y-y' phase portraits of the coupled logistic maps (a) just above the threshold of WS at $k = 0.35$ and (b) just below the threshold of WS at k=0.32.

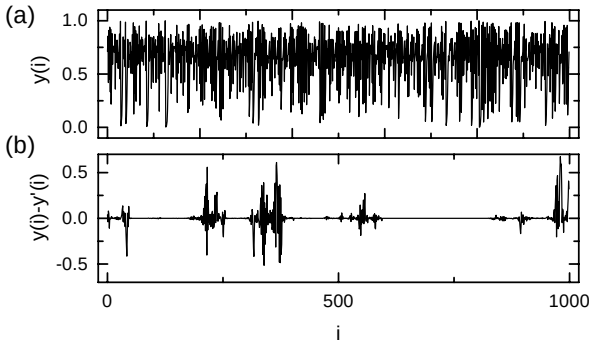

Fig. 6. (a) Dynamics of the original response system $y(i)$ and (b) the difference $y(i) - y'(i)$ just below the threshold of WS at $k = 0.33$.

just below the threshold of WS. Intermittency is not seen in the dynamics of the original response system $y(i)$ [Fig. 6(a)] but it is evident in the signal $y(i) - y'(i)$ [Fig. 6(b)] formed from the difference of the output of the original and auxiliary response systems. Recall that the auxiliary response system y' does not influence the dynamics of the original response y and driving x systems but serves only as an indicator of intermittent behavior in the x-y plane, which is related to the loss of stability of the fractal synchronization manifold.

Now let us compare this intermittent behavior with conventional on-off intermittency. Instead of investigating the escape of trajectories from a fractal synchronization manifold $y = \Phi(x)$ in the x-y plane, we can consider the escape of trajectories from the identity manifold $y = y'$ in the y-y' plane. In Sec. 1, we showed for a general case that the linear Eqs. (4) and (5) governing the evolution of the quantities $\delta Y = Y - \Phi(X)$ and $\delta Y' = Y - Y'$ are equivalent. Since the main properties of on-off intermittency are determined by these linear equations, we can analyze the system dynamics in y-y' coordinates rather than in x-y coordinates.

We calculated the dependence of the mean laminar length τ on the coupling strength k (Fig. 7) and the distribution of the laminar lengths $P(\tau)$ close to the threshold of WS (Fig. 8). The states $|y(i) - y'(i)| < 0.1$ were interpreted as laminar phases and the states $|y(i) - y'(i)| \geq 0.1$ were considered as bursts. The dependence of the inverse mean laminar phase length $1/\tau$ on the coupling strength k shows a well-defined linear part corresponding to a power law with the exponent -1 ($\tau \propto (k_w - k)^{-1}$), exactly as in conventional on-off intermittency [32]. The distribution of the laminar length $P(\tau)$ is also the same as in the case of conventional on-off intermittency. For moderate τ, it is well approximated by a power law with the exponent $-3/2$ ($P(\tau) \propto \tau^{-3/2}$), and for large τ, it has an exponential fall-off.

The identical properties of these two different intermittent processes are related to the fact that the problem of trajectory escape from a fractal synchronization manifold $y = \Phi(x)$ can be replaced by the problem of trajectory escape from a smooth manifold $y = y'$. The last problem is typical for conventional on-off intermittency. Let us consider the dynamical equation governing the difference $\delta y'(i) = y(i) - y'(i)$

$$\delta y'(i+1) = 4(1-k)(1 - 2y(i) + \delta y'(i))\delta y'(i). \tag{19}$$

The properties of the intermittent process are determined by small $|\delta y'(i)| \ll 1$, and we can rewrite Eq. (19) as $\delta y'(i+1) = z(i)\delta y'(i)$, where $z(i) = 4(1-k)(1 - 2y(i))$ is a chaotic process determined by Eqs. (8), (9). This is the standard form

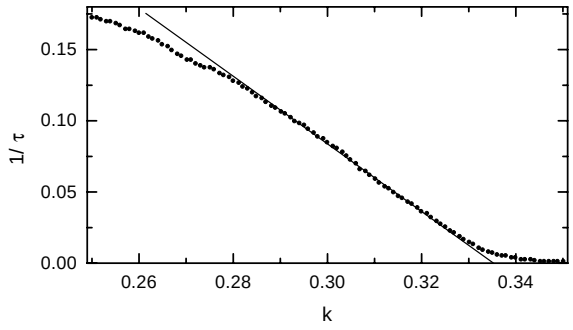

Fig. 7. Dependence of the inverse mean laminar length on the coupling strength close to the threshold of WS. For each k, a time series of 10^7 data points is used.

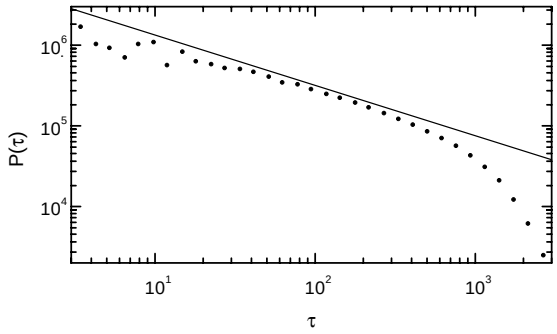

Fig. 8. Distribution of the laminar phase lengths just below the threshold of WS at $k = 0.33$. A time series of 10^7 data points is used. The solid line corresponds to a power law scaling with the exponent $-3/2$.

of a linear map driven with a chaotic signal that is considered in the theory of conventional on-off intermittency in order to derive the above properties [32].

Note that this intermittency can be considered as chaos-to-hyperchaos intermittency, since below the threshold of WS the second Lyapunov exponent of the system (8), (9) becomes positive (one Lyapunov exponent corresponds to the driving system (8); it is always positive, independent of the coupling strength k).

4. TIME SERIES ANALYSIS

In Secs. 1 and 2, we described several tools for detecting GS and analyzing its properties. The most appropriate method for experimental applications is that based on the auxiliary system approach. Unfortunately, this approach is of limited utility. The method fails for systems whose dynamical equations are not available. Even though the dynamical equations are known (e.g., in electronic circuit experiments), the auxiliary response system can be designed only with finite accuracy; it cannot be an exact copy of the original response system.

An alternative approach to detecting GS in experiments is to estimate the CLEs $\lambda_i^R, i = 1, \ldots, r$ from an observed time series [17]. Recall that the condition of GS is $\lambda_1^R < 0$; therefore, to detect GS we need to estimate only the maximal CLE. Thus, without recourse to an experimental auxiliary response system, we can predict whether an identical copy of the response system connected to the driving system will exhibit behavior identical to the original response system.

If we are interested in the properties of the synchronization manifold, we may need to estimate some additional CLEs and perhaps some of the Lyapunov exponents of the driving system $\lambda_i^D, i = 1, \ldots, d$, in order to compare the global Lyapunov dimension d_λ^G [Eq. (6)] with the driving dimension d_λ^D [Eq. (7)]. As a result of this comparison, we can distinguish between WS and SS. SS ($d_\lambda^G = d_\lambda^D$) corresponds to $\lambda_1^R < \lambda_{l_D+1}^D$. Otherwise, we have WS, $d_\lambda^G > d_\lambda^D$. Alternatively, we can evaluate the smoothness of the synchronization manifold by estimating the mean local thickness σ of the synchronization manifold. The algorithms for estimating CLEs and σ from a time series are similar. Below, we present only the algorithm for estimating CLEs.

Note that only a finite number of Lyapunov exponents can be reliably determined from data on the attractor [37]. An appropriate cut-off value for the number of exponents is related to the global Lyapunov dimension and is equal to $l_G + 1$. The only exponents that are included in Eq. (6) are fundamentally important to the character of the attractor and their estimation is available from time series. In

the case of WS, at least maximal CLE affects the global dimension, hence, it can be estimated from a time series. The condition of SS $\lambda_1^R < \lambda_{l_D+1}^D$ corresponds to the case where the global dimension d_G does not depend on the CLEs. Thus, we cannot expect a reliable estimation of CLEs from time series above the threshold of SS. However, the CLEs can be determined just before this threshold, and it suffices to estimate the characteristic values of the control parameters corresponding to the onset of SS.

Algorithm for estimating CLEs

In experiments, we generally, do not have the luxury of working with the actual vectors of phase space variables. Normally, only the time series of a single variable is available to characterize the behavior of each system. Suppose that an experimental system under investigation can be simulated by Eqs. (1), (2). We imagine that the equations are unknown, but two scalar time series x_i and y_i, $i = 1, \ldots, N$ corresponding to the driving and response subsystems, respectively, are available for observation. We assume that the time interval τ between measurements is fixed so that $x_i = x(i\tau)$ and $y_i = y(i\tau)$. In what follows, τ is identified with the delay time of phase space reconstruction in step (a) of our algorithm. In principle, any choice of τ is acceptable in the limit of an infinite amount of data. For a small amount of data, the choice of τ can be based, for example, on the evaluation of mutual information [38].

Due to the one-way coupling, the x_i series does not contain any information about the response system, while the y_i series contains information about both subsystems. Since the CLEs represent a part of the whole Lyapunov spectrum, one can expect that they can be determined by standard algorithms [37, 39, 40] from the y_i time series. However, the CLEs may be placed far from the maximal exponent in the whole Lyapunov spectrum, while standard algorithms give reliable values for only a few of the largest exponents [37, 39, 40]. Moreover, it is a nontrivial problem to define which exponents belong to the CLEs and which to the driving system, even though the whole spectrum of the Lyapunov exponents is reliably determined. These problems can be solved in the framework of an algorithm that involves information from both scalar time series x_i and y_i. Here, we mainly use the ideas of the algorithm proposed by Eckmann *et al.* [40] based on the construction of local linear maps. The mappings with a higher order Taylor series [37] are beyond our scope. We extend the Eckman-Kamphorst-Ruelle-Ciliberto (EKRC) algorithm to the case of two time series and adopt it for the direct estimation

of the CLEs. The reliability of estimating the maximal CLE by our algorithm is comparable to that of estimating the conventional maximal Lyapunov exponent by the EKRC algorithm.

To speed up the computation and to bring our consideration closer to a real experimental situation, we represent the time series x_i and y_i by integer numbers normed to the same maximal value M_0 so that $0 \leq x_i \leq M_0$ and $0 \leq y_i \leq M_0$. Typically, we take $M_0 = 10000$, in accordance with a precision of 10^{-4}. Like the EKRC algorithm, our algorithm involves the following three steps: (a) reconstructing the dynamics by the time-delay method [41] and finding the neighbors of the fiducial trajectory, (b) obtaining the tangent maps by a least-squares fit, and (c) deducing the CLEs from the tangent maps. Now let us consider these steps in detail.

(a) We choose different embedding dimensions E_x and E_y for the driving and response systems and define $(E_x + E_y)$-dimensional vectors

$$R_i = \{x_{i-E_x+1}, \ldots, x_{i-2}, x_i, y_{i-E_y+1}, \ldots, y_{i-2}, y_i\} \tag{20}$$

for $i = i_0 \equiv \max(E_x, E_y), i_0 + 1, \ldots, N$, to construct the dynamics of the fiducial trajectory in the whole $X \oplus Y$ phase space. In view of step (b), we have to determine the neighbors of R_i, i.e., the points R_j of the orbit that are contained in a ball of small radius ϵ_i centered at R_i,

$$\|R_j - R_i\| \leq \epsilon_i. \tag{21}$$

Here $\|\cdot\|$ implies the maximal projection of the vector rather than the Euclidean norm. This allows a fast search for the R_j by first sorting the data [40]. Let us denote by J_i the number of neighbors R_j of R_i within a distance ϵ_i, as determined by Eq. (21). Clearly, J_i depends on ϵ_i. In (b) we discuss the choice of these parameters for every i.

(b) Having embedded our dynamical system, we want to determine the tangent map that describes how the time evolution sends small vectors around $R_i = \{X_i, Y_i\}$ to small vectors around Y_{i+m}. This problem can be considered in a phase space of reduced dimension [40]. Following [37], we introduce local dimensions $L_x \leq E_x$ and $L_y \leq E_y$ that reflect the number of dimensions necessary to capture the geometry of a small neighborhood of the attractor after it has been successfully embedded (i.e., the time delay representation is diffeomorphic to the original attractor). The dimensions L_x and L_y are used for constructing local maps and correspond to the number of Lyapunov exponents of the driving system and the

CLEs, respectively, produced by the algorithm. The transition from embedding dimensions to local dimensions is performed as in [40]. We drop the intermediate components in Eq. (20) and define the L_x-dimensional X_i and L_y-dimensional Y_i vectors as

$$X_i = (x_{i-E_x+1}, \ldots, x_{i-m}, x_i)^T, \tag{22}$$

$$Y_i = (y_{i-E_y+1}, \ldots, y_{i-m}, y_i)^T. \tag{23}$$

The dimensions $L_x \leq E_x$ and $L_y \leq E_y$ are determined by the equalities $E_x = (L_x - 1)m + 1$ and $E_y = (L_y - 1)m + 1$, which we assume to hold for some integer $m \geq 1$. The case $m = 1$ corresponds to $L_x = E_x$, $L_y = E_y$. When $m > 1$, the dimension of the tangent map is reduced with respect to the embedding dimension; this can help to avoid spurious Lyapunov exponents [40].

The tangent map is defined by two matrices A_i and B_i, which are obtained by looking for neighbors R_j of R_i and imposing

$$A_i(X_j - X_i) + B_i(Y_j - Y_i) \approx Y_{j+m} - Y_{i+m}. \tag{24}$$

A_i is a rectangular $L_y \times L_x$ matrix and B_i is a square $L_y \times L_y$ matrix, which, in view of Eqs. (22) and (23), have the form

$$A_i = \begin{pmatrix} 0 & 0 & \cdots & 0 \\ 0 & 0 & \cdots & 0 \\ \vdots & \vdots & \vdots & \vdots \\ 0 & 0 & \cdots & 0 \\ a_1^i & a_2^i & \cdots & a_{L_y}^i \end{pmatrix}, B_i = \begin{pmatrix} 0 & 1 & 0 & \cdots & 0 \\ 0 & 0 & 1 & \cdots & 0 \\ \vdots & \vdots & \vdots & & \vdots \\ 0 & 0 & 0 & \cdots & 1 \\ b_1^i & b_2^i & b_3^i & \cdots & b_{L_y}^i \end{pmatrix}.$$

Matrix A_i contains L_x unknown elements $a_k^i, k = 1, 2, \ldots L_x$, and matrix B_i contains L_y unknowns $b_k^i, k = 1, 2, \ldots, L_y$. These $L_x + L_y$ unknowns are obtained by a least-squares fit

$$\min_{a_k^i, b_k^i} \frac{1}{J_i} \sum_{j=1}^{J_i} \|A_i(X_j - X_i) + B_i(Y_j - Y_i) - (Y_{j+m} - Y_{i+m})\|_{Euc}^2,$$

where $\|\cdot\|_{Euc}^2$ denotes the square of the Euclidean norm of the vector. This problem reduces to a set of $L_x + L_y$ linear equations in $L_x + L_y$ unknowns a_k^i, b_k^i, which we solve by the LU decomposition algorithm [42]. Obviously, this algorithm fails if the number of neighbors R_j of the fiducial point R_i is less than the number of unknowns, $J_i < L_x + L_y$. To avoid this problem, the radius ϵ_i has to be chosen to be sufficiently large. For the specific examples discussed below, we have selected

ϵ_i and J_i as follows. We count the number of neighbors J_i of R_i corresponding to increasing values of ϵ_i from a preselected sequence of possible values and stop when J_i first exceeds $J_{min} = 2(L_x + L_y)$. To speed up the calculations, we also stop the search for the neighbors when for given ϵ_i the number of neighbors exceeds the maximal value $J_{max} = 40$. Thus, for every i, J_i is in the interval $[J_{min}, J_{max}]$.

(c) Step (b) gives matrices A_i and B_i of the tangent map, which represent the reconstructed Jacobians D_xG and D_yG of Eq. (2) with respect to X and Y variables, respectively. The CLEs are determined by the product of the matrices $B_{i_0}B_{i_0+m}B_{i_0+2m}\ldots$. To extract the CLEs from this product, we use the QR decomposition technique [40, 42]. The method recursively defines an orthogonal matrix Q_l and an upper triangular matrix R_l, $l = 0, 1, \ldots L-1$, via $B_{i_0+lm}Q_l = Q_{l+1}R_{l+1}$, where Q_0 is the unit matrix. The CLEs are given by

$$\lambda_n^R m = \frac{1}{\tau L}\sum_{l=0}^{L-1} \ln(Q_l)_{nn},$$

where $K < (N - i_0)/m$ is the available number of matrices and $(Q_l)_{nn}$ is the diagonal element of the matrix Q_l. Note that in the final step we do not require knowledge of the matrix A_i. However, the use of this matrix in step (b) is necessary in order to correctly determine the tangent map (24) and, hence, the matrix B_i defining the CLEs.

Let us now illustrate our algorithm with the two specific examples presented in Sec. 2.

Examples

Coupled Hénon Maps. Let us come back to the model of identical one-way coupled Hénon maps described by Eqs. (13), (14). To test the algorithm, two scalar time series $x_1(i)$ and $y_1(i)$ were treated as experimental data. The results presented in Table correspond to the fixed value $k = 0.1$ and different values of the local dimensions L_x and L_y. For comparison, the correct values of the CLEs calculated directly from Eqs. (13), (14) and (16) at $k = 0.1$ are $\lambda_1^R \approx 0.227$ and $\lambda_2^R \approx -1.537$. For any $L_x \geq 2$ and $L_y \geq 2$, the algorithm gives two CLEs close to these correct values. If L_y is chosen correctly [i.e., equal to the dimension of the response system (14) $L_y = r = 2$], we obtain the right number of CLEs whose values weakly depend on L_x provided $L_x \geq 2$. For $L_y > 2$, the algorithm gives spurious CLEs in addition to the valid CLEs.

One way of identifying spurious exponents is to analyze the influence of external noise [37]. This is illustrated in Fig. 9. Here we have added Gaussian white noise to

L_y	L_x	λ_1^R	λ_2^R	λ_3^R	λ_4^R
2	2	0.228	-1.408		
2	3	0.224	-1.411		
2	4	0.219	-1.402		
3	2	0.462	0.203	-1.558	
3	3	0.459	0.186	-1.547	
3	4	0.489	0.178	-1.546	
4	2	0.530	0.206	-0.962	-1.629
4	3	0.512	0.189	-0.863	-1.612
4	4	0.536	0.191	-0.786	-1.613

Tab. 1. CLEs for coupled Hénon maps at $k = 0.1$ computed from $N = 50000$ data points evaluated with the sampling time $\tau = 1$. We vary the local dimensions L_x and L_y at fixed $m = 1$ so that they coincide with the embedding dimensions, $E_x = L_x$, $E_y = L_y$. The correct values of the CLEs calculated directly from Eqs. (13), (14) and (16) are $\lambda_1^R \approx 0.227$, $\lambda_2^R \approx -1.537$. For $L_y > 2$, the algorithm gives $L_y - 2$ spurious CLEs in addition to the two valid CLEs. The values corresponding to the valid CLEs are underlined.

the data points with the standard deviation σ_n. In Fig. 9(a) we used $L_x = L_y = 2$, while in Fig. 9(b) we used $L_x = L_y = 3$, which gives one spurious CLE. The spurious CLE in Fig. 9(b) decreases rapidly as the added noise is increased, going from +0.7 down to -0.9.

Fig. 10 shows a correlation between the dependence of the CLEs on the coupling strength k estimated from time series with that calculated directly from Eqs. (13), (14) and (16). Good agreement is observed for $k < k_3$, especially for the maximal CLE. For $k > k_3$, we have SS with the identical time series $y_1(i) = x_1(i)$ and the algorithm fails. This is in agreement with the general prediction that the CLEs cannot be reliably estimated from time series in the domain of SS. However, the algorithm gives the correct values of the maximal CLE in the immediate vicinity of the threshold $k \lesssim k_3$.

Coupled Rössler and Lorenz Systems. Let us now consider more complex system described by Eqs. (17), (18). In testing the algorithm, the variables $x_1(t)$ and $y_1(t)$ were treated as experimentally available outputs. The maximal CLE and the global Lyapunov dimension obtained from time series analysis are shown by dots in Figs. 4(a) and 4(b), respectively. The calculations were performed at the following values of the parameters: $N = 50000$, $\tau = 0.15$ for $k \leq 10$ and $\tau = 0.03$ for $k > 10$, $L_x = L_y = 3$, and $m = 1$. In Figs. 4(a) and 4(b), the

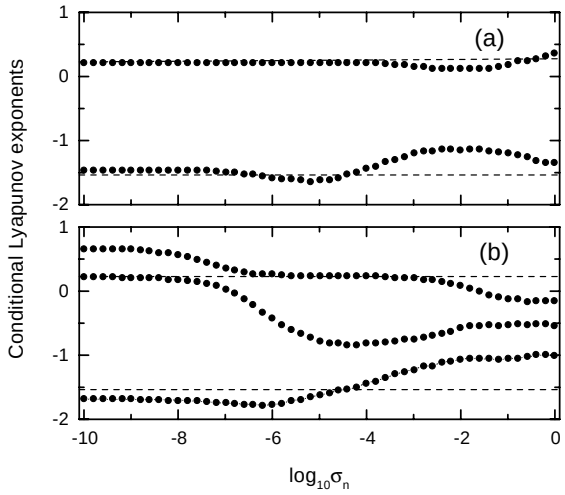

Fig. 9. The effect of external noise on the determination of the CLEs for coupled Hénon maps at the same values of parameters as in Table . σ_n is the standard deviation of the noise added to the data. (a) The local dimensions are $L_x = L_y = 2$. (b) Here $L_x = L_y = 3$. The spurious exponent wanders from about +0.7 to nearly -0.9 as the noise level is increased. The exponents do not cross each other, but switch roles as they become close. The correct values of the CLEs are shown by dashed lines.

same characteristics determined directly from Eqs. (17), (18) are shown by solid lines. Good agreement of the corresponding characteristics is observed in a large interval of the coupling strength k. Thus, the results of the time series analysis allow us to correctly predict both the threshold of GS and the smoothness of the synchronization manifold.

5. CONCLUSIONS

The generalized synchronization of chaos is a natural generalization of the concept of identical synchronization to the case of nonidentical chaotic systems. This phenomenon is typical for one-way coupled chaotic systems. It appears, when under the action of the driving system, the response system "forgets" its initial conditions and becomes an asymptotically stable system, i. e., when any initial conditions in the response lead to the same asymptotic dynamics. Physically, this means that an ensemble of identical response systems driven with the same chaotic signal should exhibit identical asymptotic behavior. This resembles the well-known

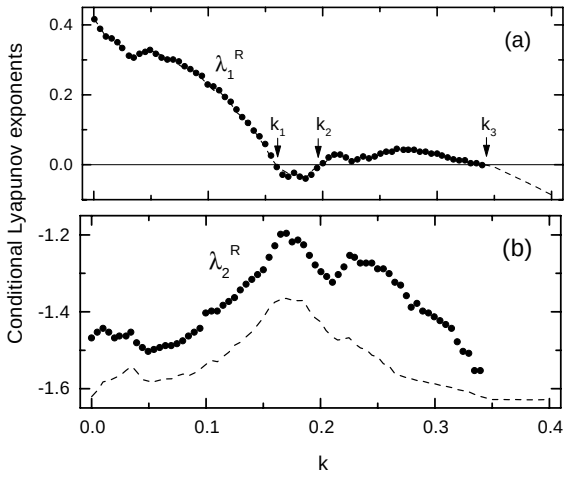

Fig. 10. Dependence of the CLEs on the coupling strength for coupled Hénon maps at $m = 1$, $L_x = L_y = 2$. The points correspond to the values of the CLEs estimated from time series and the dashed lines show the correct values of the CLEs calculated directly from Eqs. (13), (14) and (16).

physical phenomenon known as the bunching or grouping effect, which is widely used in particle accelerators and other similar systems. Here an ensemble of identical particles started from different initial conditions is grouped to a common trajectory. The difference is that in the bunching effect one usually takes a periodic driving signal; in generalized synchronization, however, we consider chaotic driving. The parallel with the bunching phenomenon makes evident the idea of the auxiliary system approach. To detect the bouncing phenomenon or generalized synchronization, one requires an ensemble of identical response systems. This ensemble should consist of at least of two identical systems, namely, the original and the auxiliary response systems.

In the phase space interpretation, the asymptotical stability of the response system leads to a stable synchronization manifold $M = \{(X, Y) : \Phi(X) = Y\}$ that relates the variables of the driving and the response systems. Depending on the coupling strength, the generalized synchronization appears as weak synchronization or strong synchronization. Weak synchronization is characterized by a fractal manifold M with a nonsmooth map Φ that increases the global dimension with respect to the dimension of the driving system, $d^G > d^D$. Strong synchronization

is related to a smooth map Φ so that the response system does not influence the global dimension, $d^G = d^D$. The threshold of generalized synchronization, in addition to certain properties of the synchronization manifold, can be expressed through the conditional Lyapunov exponents λ_i^R and the Lyapunov exponents of the driving system λ_i^D. The mean local thickness σ of the synchronization manifold can be used as an alternative characteristic to estimate the smoothness of the manifold.

The onset of generalized synchronization is characterized by a new type of on-off intermittency. Unlike the conventional situation, this intermittency can occur in nonsymmetrical systems that do not possess any trivial invariant manifolds. It may appear in any system consisting of two one-way coupled chaotic subsystems. The intermittent behavior appears just below the threshold of weak synchronization and is determined by the loss of stability of the invariant fractal synchronization manifold. It is not noticeable in the phase space of the original response and driving systems; however, it can be detected and analyzed with the help of an auxiliary response system.

In experiment, two alternative tools can be used to detect and analyze the generalized synchronization of chaos. One of these is based on an auxiliary response system. Here, the experimental situation should admit the design of a replica of the response system. Another approach is based on time series analysis. Using two scalar time series, one taken from the driving system and the other from the response system, one can estimate the conditional Lyapunov exponents and other parameters that define the existence and the properties of generalized synchronization. The both approaches we have successfully tested for electronic circuit experiments described in [43]. We have analyzed generalized synchronization in two one-way coupled identical double-scroll chaos oscillators and in a double-scroll chaos oscillator driven with electronic analog of a Mackey-Glass system.

REFERENCES

1. S. Hayes, C. Grebogy, E. Ott, *Phys. Rev. Lett.,* **70**, p. 3031, 1993;
   K. M. Cuomo, A. V. Oppenheim, *Phys. Rev. Lett.,* **71**, p. 65, 1993;
   T. Kapitaniak, *Phys. Rev.* E, **50**, p. 1642, 1994;
   G. Perec, H. A. Cerdeira, *Phys. Rev. Lett.,* **74**, p. 1970, 1995;
   J. H. Peng, E. J Ding, M. Ding, W. Yang, *Phys. Rev. Lett.,* **76**, p. 904, 1996.

2. K. Pyragas, *Phys. Lett.* A, **181**, p. 203, 1993.

3. A. Kittel, K. Pyragas, R. Richter, *Phys. Rev.* E, **50**, p. 262, 1994.

4. R. Brown, N. F. Rulkov, E. R. Tracy, *Phys. Rev.* E, **49**, p. 3784, 1994.

5. U. Parlitz, *Phys. Rev. Lett.,* **76**, p. 1232, 1996.

6. H. G. Winful, L. Rahman, *Phys. Rev. Lett.,* **65**, p. 1575, 1990.

7. P. V. Bayly, E. E. Johnson, P. D. Wolf, H. S. Greenside, W. M. Smith, R. E. Ideker, *J. Cardiovas. Electrophysiol.,* **4**, p. 533, 1993.

8. L. M. Pecora, T. L. Carrol, *Phys. Rev. Lett.,* **64**, p. 821, 1990.

9. H. Fujisaka, T. Yamada, *Prog. Theor. Phys.,* **69**, p. 32, 1983;
T. L. Carrol, *Phys. Rev.* E, **50**, 2580, 1994.

10. L. Kocarev, U. Parlitz, *Phys. Rev. Lett.,* **76**, p. 1816, 1996.

11. M. G. Rosenblum, A. S. Pikovsky, J. Kurths, *Phys. Rev. Lett.,* **76**, p. 1804, 1996.

12. V. S. Afraimovich, N. N. Verichev, M. I. Rabinovich, *Radiophys. Quantum Electron.,* **29**, p. 795, 1986.

13. N. F. Rulkov, M. M. Sushchik, L. S. Tsimring, H. D. I. Abarbanel, *Phys. Rev.* E, **51**, p. 980, 1995.

14. H. D. I. Abarbanel, N. F. Rulkov, M. M. Sushchik, *Phys. Rev.* E, **53**, p. 4528, 1996.

15. N. F. Rulkov, M. M. Sushchik, *Phys. Lett.* A, **214**, 145, 1996;
N. F. Rulkov, *Chaos,* **6**, p. 262, 1996.

16. K. Pyragas, *Phys. Rev.* E, **54**, R4508, 1996.

17. K. Pyragas, *Phys. Rev.* E, **56**, p. 5183, 1997.

18. K. Pyragas, *Chaos, Solitons and Fractals,* **9**, p. 337, 1998.

19. L. M. Pecora, T. L. Carrol, *Phys. Rev.* A, **44**, p. 2374, 1991.

20. L. Yu, E. Ott, Q. Chen, *Phys. Rev. Lett.,* **65**, p. 2935, 1990;
A. S. Pikovsky, *Phys. Lett.* A, **165**, p. 33, 1992.

21. M. Ding, C. Grebogi, E. Ott, T. Sauer, J. A. Yorke, *Physica* D, **69**, p. 404, 1993.

22. T. Sauer, J. A. Yorke, *Ergodic Theory Dyn. Syst.,* (to appear).

23. J. L. Kaplan, J. A. Yorke, *In: Functional Differential Equations and Approximation of Fixed Points,* eds. H.-O. Peitgen and H.-O. Walther, Springer Lecture Notes in Mathematics, Vol. **730**, (Springer, Berlin) p. 204, 1979.

24. R. Badii, G. Broggi, B. Derighetti, M. Ravani, S. Ciliberto, A. Politi, M. A. Rubio, *Phys. Rev. Lett.,* **60**, p. 979, 1988.

25. P. Grassberger, I. Procaccia, *Phys. Rev. Lett.,* **50**, p. 346, 1983.

26. M. Hénon, *Math. Phys.,* **50**, p. 69, 1969.

27. O. E. Rössler, *Phys. Lett.* A, **57**, p. 397, 1976.

28. E. N. Lorenz, *J. Atmos. Sci.,* **20**, p. 130, 1963.

29. N. Platt, E. A. Spiegel, C. Tresser, *Phys. Rev. Lett.,* **70**, p. 279, 1993.

30. E. Ott, J. Sommerer, *Phys. Lett.,* **188**, p. 39, 1994.

31. A. S. Pikovsky, *Z. Phys.* B, **55**, p. 149, 1984;
H. Fujisaka, H. Yamada, *Prog. Theor. Phys.* **74**, p. 918, 1985;
75, p. 1087, 1986.

32. J. F. Heagy, N. Platt, S. M. Hammel, *Phys. Rev.* E, **49**, p. 1140, 1994.

33. H. L. Yang, E. J. Ding, *Phys. Rev.* E, **50**, R3295, 1994.

34. J. C. Sommerer, E. Ott, *Nature,* **365**, p. 138, 1993;
E. Ott, J. C. Sommerer, *Phys. Lett.* A, **188**, p. 39, 1994.

35. J. F. Heagy, T. L. Carrol, L. M. Pecora, *Phys. Rev. Lett.,* **73**, p. 3528, 1994;
P. W. Hammer, N. Platt, S. M. Hammel, J. F. Heagy, B. D. Lee, *Phys.Rev.Lett.,* **73**, p. 1095, 1994;
T. Kapitaniak, J. Phys. A, **28**, L63, 1995;
Y. H. Yu, K. Kwak, T. K. Lim, *Phys. Lett.* A, **198**, p. 34, 1995;
A. Čenys, A. Namajūnas, A. Tamaševičius, T. Schneider, *Phys. Lett.* A, **213**, p. 259, 1996.

36. F. Rodelsperger, A. Čenys, H. Benner, *Phys. Rev. Lett.,* **75**, p. 2594, 1994.

37. P. Bryant, R. Brown, H. D. I. Abarbanel, *Phys. Rev. Lett.,* **65**, p. 1523, 1990;
R. Brown, P. Bryant, H. D. I. Abarbanel, *Phys. Rev.* A, **43**, p. 2787, 1991.

38. A. M. Fraser, H. L. Swinney, *Phys. Rev.* A, **33**, p. 1134, 1986.

39. A. Wolf, J. B. Swift, H. L. Swinney, J. A. Vastano, *Physica* D, **16**, p. 285, 1985.

40. J.-P. Eckmann, S. O. Kamphorst, D. Ruelle, S. Ciliberto, *Phys. Rev.* A, **34**, p. 4971, 1986.

41. N. H. Packard, J. P. Crutchfield, J. D. Farmer, R. S. Shaw, *Phys. Rev. Lett.,* **45**, p. 712, 1980.

42. W. H. Press, S. A. Teukolsky, W. T. Vetterling, B. P. Flannery, *Numerical Recipes in C, The Art of Scientific Computing,* Second Edition, Cambridge University Press, Cambridge, 1994.

43. A. Kittel, J. Parisi, K. Pyragas, *Physica* D, **112**, p. 459, 1998.